Journal of Crystal Growth 349 (2012) 43–49

Contents lists available at SciVerse ScienceDirect

Journal of Crystal Growth

journal homepage: www.elsevier.com/locate/jcrysgro

Doping induced lattice misfit in 4H–SiC homoepitaxy

Birgit Kallinger [a,*], Patrick Berwian [a], Jochen Friedrich [a], Georg Müller [a,b], Arnd-Dietrich Weber [c], Eduard Volz [c], Gerd Trachta [c], Erdmann Spiecker [d], Bernd Thomas [e,1]

[a] Department of Crystal Growth, Fraunhofer IISB, Schottkystr. 10, 91058 Erlangen, Germany
[b] Crystal Consulting, Birkenstr. 17, 91094 Langensendelbach, Germany
[c] SiCrystal AG, Thurn-und-Taxis-Str. 20, 90411 Nürnberg, Germany
[d] Center of Nanoanalysis and Electron Microscopy (CENEM), Department of Material Sciences, University of Erlangen-Nürnberg, Cauerstr. 6, 91058 Erlangen, Germany
[e] SiCED Electronics Development, Günther-Scharowsky-Str. 1, 91058 Erlangen, Germany

ARTICLE INFO

Article history:
Received 7 December 2011
Received in revised form
21 March 2012
Accepted 30 March 2012
Communicated by M. Skowronski
Available online 7 April 2012

Keywords:
A1. Defects
A1. Stresses
A1. X-ray diffraction
A3. Chemical vapor deposition
B1. Silicon carbide

ABSTRACT

The impact of doping on the lattice constants of 4H–silicon carbide (4H–SiC) is an important material aspect influencing several steps of material and device production. Dopant incorporation in 4H–SiC causes misfit between the highly N-doped substrate and differently doped epilayers and hence, wafer bowing and the existence of a critical epilayer thickness. In this paper, the wafer bow is determined by geometrical measurements of the substrate prior to and after the epitaxial growth of single epilayers with different epilayer thicknesses and doping states, i.e. with nitrogen (N) or aluminum (Al) doping and different dopant concentrations. The misfit between substrate and epilayer is deduced from these bow measurements based on a model by Stoney. For highly Al-doped epilayers grown on highly N-doped substrates, the misfit is determined additionally by HRXRD measurements. The doping-dependent misfit, obtained from bow and HRXRD measurements, is compared to theoretical values calculated based on a model by Jacobson. For Al-doped epilayers, the experimental and theoretical values of misfit agree well. For N-doped epilayers, an effective covalent radius of N in 4H–SiC of 66 pm has to be introduced to match the theoretical misfit to the experimental one. The critical epilayer thickness is calculated based on the models by Matthews and Blakeslee and by People and Bean. The comparison of calculated values and experimental findings with respect to dislocation behavior at the substrate–epilayer interface and the dislocation densities of epilayers proves that the model by Matthews and Blakeslee underestimates the critical epilayer thickness for 4H–SiC homoepitaxy.

1. Introduction

The impact of the doping state, i.e. the doping element nitrogen (N) or aluminum (Al) and the dopant concentration, on the lattice constants of 4H–silicon carbide (4H–SiC) is an important material aspect with extensive consequences for homoepitaxial growth and for device production. For example, the structural quality of homoepitaxial layers may suffer from doping induced strain, wafer bowing and consequently, from the existence of a critical epilayer thickness. The latter one may lead to an increasing dislocation density in the epilayer due to the generation of misfit dislocations. In the case of 4H–SiC homoepitaxial growth on vicinal, (0001) oriented substrates, the in-plane lattice parameter and hence, the Burgers vector of misfit dislocations is of type $\langle 11\bar{2}0 \rangle$. Additionally, the line vector of misfit dislocations needs to be within the interface, i.e. the basal plane. Therefore, misfit dislocations in 4H–SiC homoepitaxy are basal plane dislocations (BPDs). This type of dislocation is suspected to trigger the electrical degradation of bipolar devices [1]. Furthermore, the wafer bow may cause problems with lithographic structuring during device production [2].

The lattice misfit between 4H–SiC substrate and homoepitaxial layer was already investigated for highly Al-doped epilayers grown on high purity, semi-insulating (HPSI) substrates [3], for N-doped epilayers on highly N-doped substrates [4,5] and for highly N-doped epilayers on Al-doped substrates [6] by high resolution X-ray diffraction (HRXRD). The critical epilayer thickness was experimentally determined for highly Al-doped epilayers grown on HPSI substrates [3] as well as for N-doped epilayers grown on highly N-doped substrates [5].

The aim of this paper is to assess the lattice misfit in 4H–SiC homoepitaxy by complementary experimental techniques, i.e. HRXRD and bow measurements, as well as by the model by Jacobson [5] and to study its impact on critical epilayer thickness. Therefore, N- and Al-doped homoepitaxial layers are grown on commercially available highly N-doped substrates and characterized

* Corresponding author. Tel.: +49 9131 761 273; fax: +49 9131 761 280.
E-mail address: birgit.kallinger@iisb.fraunhofer.de (B. Kallinger).
[1] Present address: Dow Corning Semiconductor Solutions, 5300 Eleven Mile Road, Auburn, MI 48611, USA.

0022-0248/$ - see front matter © 2012 Elsevier B.V. All rights reserved.
http://dx.doi.org/10.1016/j.jcrysgro.2012.03.057

with respect to the wafer curvature (bow measurements) and the lattice parameters (HRXRD). These experimental results are converted to misfit data and used to calculate the critical epilayer thickness based on two pertinent models. It will be discussed which model is appropriate for 4H–SiC homoepitaxial growth and the model predictions will be compared to experimental results.

2. Experimental

2.1. Description of samples

Homoepitaxial layers were grown on vicinal 4H–SiC substrates by chemical vapor deposition (CVD) using a horizontal hot-wall Epigress VP508 reactor equipped with Gas Foil Rotation (GFR) [7]. The 3 in substrates, provided by SiCrystal AG, were 4° off-cut towards [11$\bar{2}$0] direction and epi-ready polished on the (0001)Si face. Thin substrates with a thickness of 250 μm were chosen as it is expected that wafer bowing is more pronounced for use of thin substrates instead of thick (350 μm) substrates and hence, to improve the precision of geometry measurements. The nitrogen (N) concentration (c_N) of the substrates was determined by secondary ion mass spectroscopy (SIMS) at different lateral positions. The N concentration amounted to $c_N = 1.1 \times 10^{19}$ cm^{-3} and $c_N = 1.7 \times 10^{19}$ cm^{-3} outside and inside the facet area, respectively. For each epigrowth series, several adjacent wafers cut from one boule were used, i.e. the substrates show comparable dislocation densities and spatial distributions.

In the CVD growth process, silane and propane acted as precursors and hydrogen as carrier gas. The epilayers were doped either with nitrogen (N) or aluminum (Al) to obtain n- or p-type epilayers, respectively. All epilayers were grown at a growth temperature of T=1650 °C and a growth rate of 13 μm/h. The dopant concentration (c_N or c_{Al}) of epilayers was determined by SIMS. Measurements at different lateral positions of each epilayer confirmed that the doping homogeneity amounted to $\sigma/\text{mean} \leq 8\%$ as described in [7]. Depth profiles revealed constant dopant concentration for epilayers. The epilayer thickness was determined by Fourier transformed infrared spectroscopy (FTIR) and geometry measurements (see also Section 2.2).

Three different epigrowth series (A–C) were performed: in series A, three single epilayers were grown on three different substrates with an epilayer thickness of 12.5 μm, 25 μm and 50 μm, i.e. the epilayer thickness was doubled two times. The nitrogen doping concentration of these epilayers was kept constant at $c_N \approx 10^{15}$ cm^{-3}. In series B, the nitrogen doping concentration of different epilayers was varied from 10^{15} cm^{-3} to 2×10^{19} cm^{-3} while keeping the epilayer thickness of 10 μm constant. In series C, epilayers with different aluminum concentrations from $c_{Al} = 2 \times 10^{19}$ cm^{-3} to $c_{Al} = 1.5 \times 10^{20}$ cm^{-3} were grown. All epilayers of series C were 12.5 μm thick. The details of epilayer thickness and doping are summarized in Table 1.

2.2. Wafer geometry measurements and Stoney's model

The wafer geometry, especially the bow, was investigated by non-contact, optical bow measurements with a Precitec NEMESIS

Table 1
Dopants, their concentrations and the thicknesses of epilayers, which are grown on 4° towards [11$\bar{2}$0] off-cut substrate with substrate thickness of 250 μm. All substrates are highly N-doped with $c_N = 2 \times 10^{19}$ cm^{-3}.

Series	Dopant	Dopant concentration (cm^{-3})	Thickness h_f (μm)
A	N	10^{15}	12.5/25/50
B	N	10^{15} to 2×10^{19}	10
C	Al	2×10^{19} to 1.5×10^{20}	12.5

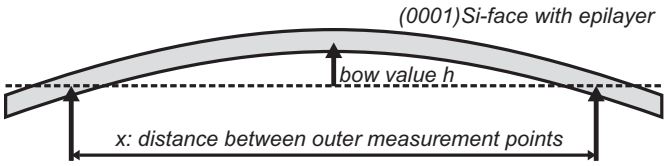

Fig. 1. Setup for bow measurement: the local position of the wafer is determined at two outer measurement points with distance x. The local height at these positions is fitted as shown by the dotted line. In the wafer center, the local height is measured with respect to the dotted line, representing the bow h.

WT based on SEMI norms MF534 and MF1390. Prior to epitaxial growth, the substrate's thickness h_s, bow h_{sub} and warp values were determined. The geometric setup for bow measurements is shown in Fig. 1. The bow was measured parallel and perpendicular to the main flat of the wafers. These geometry measurements were repeated after epitaxial growth, i.e. the latter measurement results represent the substrate–epilayer system. In order to obtain the epilayer thickness h_f and the epitaxially induced bow h, the results of the substrate were subtracted from those of the substrate–epilayer system. It is known from basic geometry that the radius of a circular segment, i.e. the curvature radius κ^{-1} of the wafer, can be calculated according to Eq. (1)

$$\kappa^{-1} = \frac{x^2}{8h} + \frac{h}{2} \tag{1}$$

with h is the epitaxially induced bow; x is the distance between the outer measurement points.

Eq. (1) is only valid if the sample exhibits a homogenous curvature. Therefore, samples with large warp values and/or deviating bow values parallel and perpendicular to the main flat were excluded from further analysis. The epitaxially induced curvature κ of each sample will be shown in Section 3.2. Furthermore, the misfit between substrate and epilayer can be determined from bow measurements based on Stoney's model [8]. It correlates the macroscopic curvature κ and the misfit ϵ between substrate and epilayer for homogeneous, biaxial isotropic strain. The strain distribution is sufficiently homogenous for all samples which passed the warp and bow criteria described above. For homoepitaxial growth, equal elastic properties e.g. elastic constants and biaxial moduli are assumed for substrate and epilayer, resulting in a more simple form of Stoney's equation (Eq. (2))

$$\epsilon = \frac{\kappa \cdot h_s^2}{6h_f} \tag{2}$$

with h_s is the substrate thickness; h_f is the epilayer thickness.

The results of the wafer geometry measurements were cross-checked by using conventional methods, i.e. the lateral homogeneity of wafer bowing as well as the bow value itself were proven by profilometer measurements. The values for epilayer thickness, deduced from repeated geometry measurements prior and after epitaxial growth, fit very well to FTIR measurement results. Therefore, systematic errors of geometry measurements are negligible. Furthermore, the statistical error of the geometry measurements and subsequent analysis of the results according to Eqs. (1) and (2) was calculated based on the propagation of uncertainty. The statistical error of this analysis is smaller by two orders of magnitude than the results of the analysis, i.e. the curvature κ and the misfit ϵ. Therefore, no error bars are given for curvature κ and misfit ϵ deduced from geometry measurements. The detection limit of geometry measurements regarding the misfit can be calculated based on Eqs. (1) and (2) and typical geometry data. Assuming a minimum bow of $h_{min} = 0.3$ μm, x=60 mm, $h_s = 250$ μm and $h_f = 10$ μm, the detection limit regarding the misfit is about 7×10^{-7}.

2.3. Analysis of reciprocal space maps

High resolution X-ray diffraction (HRXRD) was used to determine the lattice constants of substrate and epilayer and to distinguish between pseudomorphic and relaxed epigrowth. Reciprocal space maps (RSM) were recorded on (0008) and ($10\bar{1}8$) reflections with a PANalytical X'Pert MRD in triple axis setup, i.e. the intensity distribution in reciprocal space around these basic reflections is monitored by series of ω-2θ-scans with successively increasing ω. In case that peak splitting occurs as shown in Fig. 2, the substrate and epilayer peak can be identified by their relative intensities and angular positions [3]. The determination of lattice parameters and misfit consists of the following steps: first, the 2θ angular positions of substrate and epilayer peak are extracted from the RSM on the (0008) reflection and converted to d-spacings based on Bragg's equation. The c-lattice parameter of the substrate (c_0) and the strained lattice parameter c_f of the epilayer can be calculated from the d-spacings. The a-lattice constants of substrate (a_0) and strained epilayer (a_f) can be determined from the RSM on the ($10\bar{1}8$) reflection analogously. Second, the strained lattice parameters a_f and c_f of the epilayer are converted to relaxed lattice parameters a_r and c_r based on Eqs. (3) and (4) given in [3]. Third, the relaxed lattice parameters are used to calculate the lattice misfit ϵ by Eq. (3)

$$\epsilon = \frac{a_0 - a_r}{a_r}. \tag{3}$$

RSMs were measured several times for each sample at different positions, i.e. at the center of the wafer and at half of the wafer radius, in order to calculate the mean values and deviation of strained lattice parameters. The systematic and statistical errors caused by the measurement method and setup are small compared to errors caused by material inhomogeneity, e.g. the lateral variation of the epilayer's dopant concentration and thickness.

2.4. Synchrotron X-ray topography and defect selective etching

The dislocation content of substrates and epilayers was determined by defect selective etching (DSE) and synchrotron X-ray topography (SXRT). DSE was carried out in molten potassium hydroxide (KOH) at 520 °C for several minutes in order to obtain the etch pit density (EPD). It was proven in [9] that the dislocation density and the EPD at the sample surface coincide.

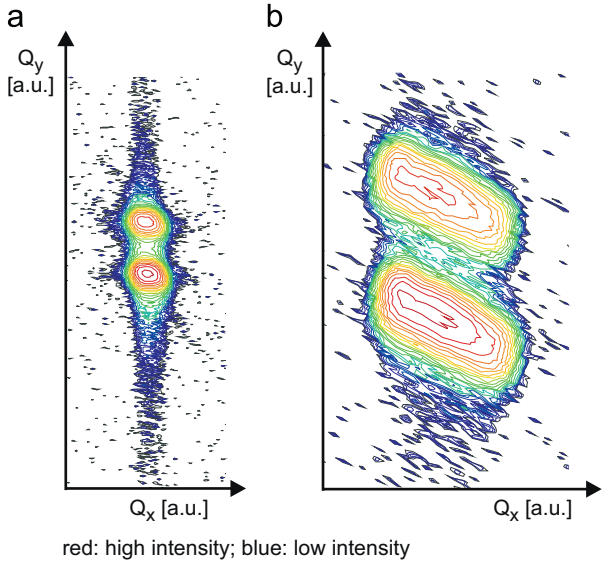

Fig. 2. Reciprocal space maps of (0008) and ($10\bar{1}8$) reflections from Al-doped epilayer ($c_{Al} = 1.5 \times 10^{20}$ cm^{-3}) grown on highly N doped substrate.

White beam SXRT was performed at the Angstromquelle Karlsruhe (ANKA) [10]. SXRT was performed in back reflection geometry in order to investigate dislocations close to the sample surface as described in [9]. Appropriate diffraction conditions were chosen to adapt the information depth in topographs to the epilayer thickness, i.e. for the detection of potential misfit dislocations at the substrate–epilayer interface.

3. Results

3.1. Dislocation densities of substrates and epilayers

The dislocation density at the sample surface, i.e. the etch pit density (EPD), was obtained by defect selective etching. All epilayers from one epigrowth series, i.e. epilayers grown on adjacent substrates cut from one boule, contain a comparable amount of dislocations in the order of low 10^4 cm^{-2} and show comparable spatial distribution of dislocations.

Furthermore, dislocations were tracked from the substrate to the subsequently grown epilayer by comparison of respective SXRT topographs. Such dislocation tracking reveals that the total dislocation densities of substrate and subsequently grown epilayer are identical as described in [11] because threading dislocations (e.g. TED, TSD) propagate from the substrate to the epilayer and BPDs from the substrate can either propagate as BPDs or convert to TEDs in the epilayer. This investigation proves that dislocations are neither stopped or trapped nor generated at the substrate–epilayer interface. Furthermore, no stacking faults are present in the substrates or epilayers. More details on dislocation behavior during homoepitaxial growth will be published elsewhere [12].

3.2. Determination of wafer curvature

The measured values of epitaxially induced bow h are converted to curvature κ according to Eq. (1). All epilayers exhibit a convex curvature. The influence of the epilayer doping on curvature is shown in Fig. 3a: for Al-doped epilayers grown on highly N-doped substrates (series C), the curvature increases with increasing Al concentration. For N-doped epilayers (series B), the curvature is smaller than for Al-doped epilayers. In case of low N-doped epilayers with $c_N < 5 \times 10^{17}$ cm^{-3}, the curvature is constant at a value of $\kappa \approx 0.02$ m^{-1}. For epilayers with N concentrations in the range of 5×10^{18} cm^{-3} $< c_N < 2 \times 10^{19}$ cm^{-3}, the curvature decreases significantly within the measurement accuracy.

In Fig. 3b, the dependence of curvature on the epilayer thickness is shown for low N-doped layers with $c_N \approx 10^{15}$ cm^{-3} (series A). The curvature increases linearly to the epilayer thickness.

3.3. Determination of lattice constants by HRXRD

Reciprocal space maps (RSM) were measured on all samples. Only for Al-doped epilayers with $c_{Al} \geq 6.5 \times 10^{19}$ cm^{-3}, peak splitting is observed as shown in Fig. 2. As described in Section 2.3, strained lattice constants of the Al-doped epilayers were deduced from RSMs. The a-lattice parameters of substrates (a_0) and strained epilayers (a_f) are shown in Fig. 4a as a function of the epilayers' Al-concentration. The mean value of all a-lattice parameters $\bar{a} = 0.30815$ nm is displayed as a dotted line. One can clearly see that the a-lattice parameters of substrates and strained epilayers agree well and are independent of the Al-concentration in the epilayer.

In Fig. 4b, the c-lattice parameters of substrate (c_0) and strained epilayer (c_f) are plotted versus the epilayers' Al-concentration. The c-lattice parameter of substrates remains constant at

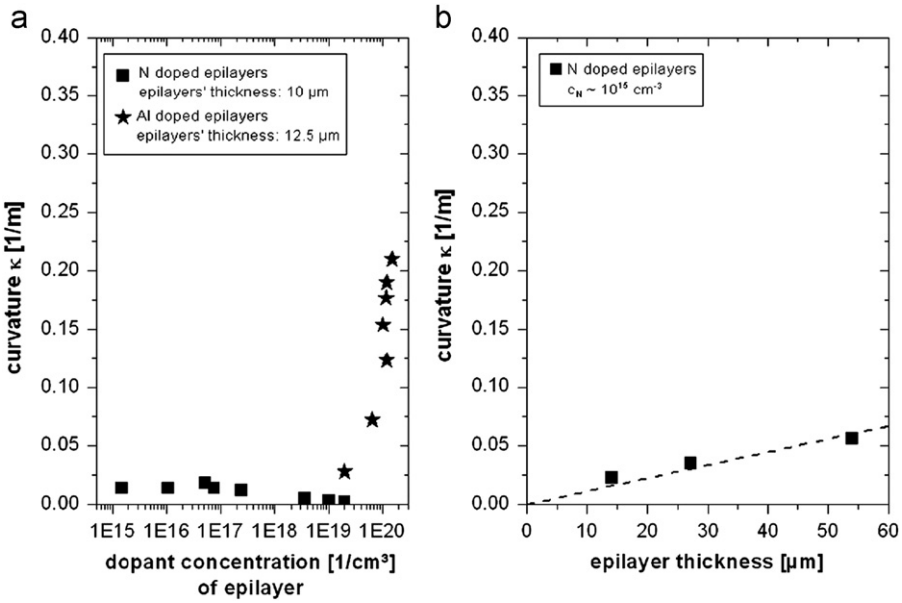

Fig. 3. Curvature of samples as a function of dopant and dopant concentration (a, series B and C) and epilayer thickness (b, $c_N = 10^{15}$ cm^{-3}, series A).

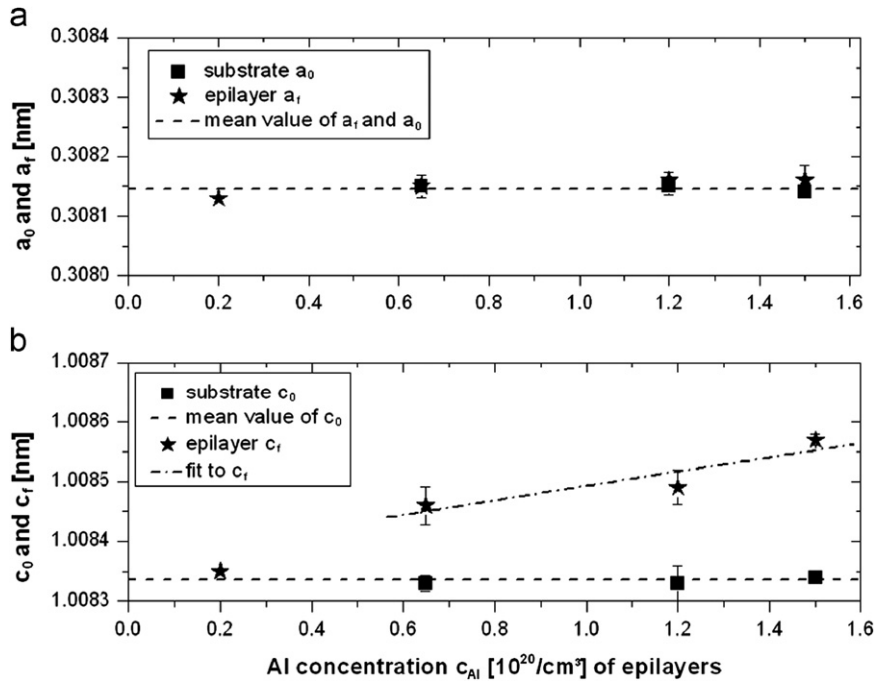

Fig. 4. Experimental lattice constants for N-doped substrates and Al-doped epilayers as a function of the epilayers' Al-concentration obtained from RSMs. (a) a-lattice constants of substrate (a_0) and strained epilayer (a_f). The mean value of all a-lattice constants of substrates and epilayers is displayed as dotted line. (b) c-lattice parameters of substrates (c_0) and Al-doped epilayers (c_f). The mean value of c_0 is plotted as dotted line. A least squares fit to the strained c-lattice parameter of epilayers is given as point-dot-line.

$c_0 = 1.00834$ nm. Contrary to that, the strained c-lattice parameter c_f of the Al-doped epilayers increases with increasing Al-concentration of the epilayer for $c_{Al} \geq 6.5 \times 10^{19}$ cm^{-3}. For $c_{Al} < 6.5 \times 10^{19}$ cm^{-3}, the c-lattice parameters of substrate and strained epilayer are identical ($c_0 = c_f$) within experimental accuracy as no peak splitting occurs.

Finally, the relaxed lattice parameters a_r and c_r of the epilayers are calculated from the strained lattice parameters a_f and c_f as described in Section 2.3. The results are given in Table 2.

Table 2
Relaxed lattice parameters of 4H–SiC as a function of Al-concentration. The relaxed lattice parameters are calculated from strained lattice parameters (mean values of repeated measurements) according to Eqs. (3) and (4) given by Huh et al. [3].

c_{Al}(10^{20} cm^{-3})	0.2	0.65	1.2	1.5
a_r (nm)	0.30815	0.30818	0.30819	0.30820
c_r (nm)	1.00834	1.00845	1.00848	1.00853

The relaxed lattice parameters, which represent the equilibrium case or free-standing material with the given Al-concentration, are increasing with increasing Al content. Contrary to the strained a-lattice parameter a_f given in Fig. 4, the relaxed a-lattice constant a_r is also increasing with Al-concentration. The increase of the relaxed c-lattice parameter c_r is less pronounced than for strained c-lattice parameters c_f.

4. Discussion

In the first part of the discussion, the lattice misfit between highly N-doped substrates and epilayers will be determined from experimental data of bow and HRXRD measurements. These experimentally derived data will be compared to theoretical values to deduce the origin of misfit. In the second part of the discussion, these misfit values will be used to calculate the critical epilayer thickness in dependence of the epilayer's doping based on two pertinent models. Finally, the model predictions will be compared to experimental results.

4.1. Lattice misfit between substrate and epilayer

The lattice misfit between substrate and epilayer can be deduced from bow and HRXRD measurements, which are shown in Section 3. The bow values can be converted to misfit data according to Stoney's model [8], i.e. Eq. (2). Furthermore, the misfit can be deduced from relaxed lattice parameters of substrate and epilayer based on Eq. (3). Additionally, the theoretical misfit can be predicted based on Jacobson's model [5]. This model assumes that host atoms are substituted by dopant atoms. The size, i.e. the covalent radius, of host and dopant atoms is deviating, resulting in a relative change of lattice parameters depending on the substituent and its concentration c_s. It is known that carbon (C) host atoms with a covalent radius of 77 pm [13] are substituted by nitrogen (N) atoms with a covalent radius in the range of 70 pm [13] up to 75 pm [14]. As N atoms have a slightly smaller covalent radius than C atoms, lattice contraction is expected for N doping. Silicon (Si) host atoms are replaced by aluminum (Al) atoms, having covalent radii of 117 pm [13] and 125 pm [13], respectively. Consequently, Al incorporation on Si lattice sites leads to dilatation of the 4H–SiC lattice. Jacobson et al. [5] have shown that the relative, isotropic change f in lattice parameters can be calculated as

$$f = \frac{4\pi}{3}(r_s^3 - r_h^3)\cdot c_s \cdot \frac{3K+4G}{9K}, \tag{4}$$

with c_s is the concentration of substituent; r_s and r_h are the covalent radius of substituent and host atom, respectively; K is the bulk modulus, $K=221$ GPa [15]; G is the shear modulus, $G=159$ GPa [15].

The misfit between a highly N-doped substrate with $c_N = 2\times 10^{19}$ cm^{-3} and an epilayer with a certain dopant and its concentration can be calculated as

$$\epsilon = |f_s - f_f|. \tag{5}$$

The experimental results and the model prediction regarding misfit ϵ are plotted versus the doping concentration of the epilayer in Fig. 5. All the experimental data and the theoretical prediction indicate compressive strain for N doped as well as for Al-doped epilayers grown on highly N-doped substrates, i.e. the relaxed lattice constants of all epilayers need to be larger than those of the substrate. Highly N-doped substrates do have the smallest lattice constants within the investigated doping range as (i) N doping contracts the 4H–SiC lattice and (ii) substrates possess the largest N concentration. As N-doped epilayers have lower N concentrations than the substrates, the N-doped epilayers have slightly larger lattice constants than the substrates. Doping with Al dilates the 4H–SiC lattice due to the larger covalent radius of Al atoms than of Si atoms, which is consistent with our experimental results (compare also Table 2). Therefore, all Al-doped epilayers possess larger lattice constants than the highly N-doped substrates. In summary, all epilayers exhibit larger relaxed lattice constants than the highly N-doped substrates, resulting in compressive strain in all epilayers.

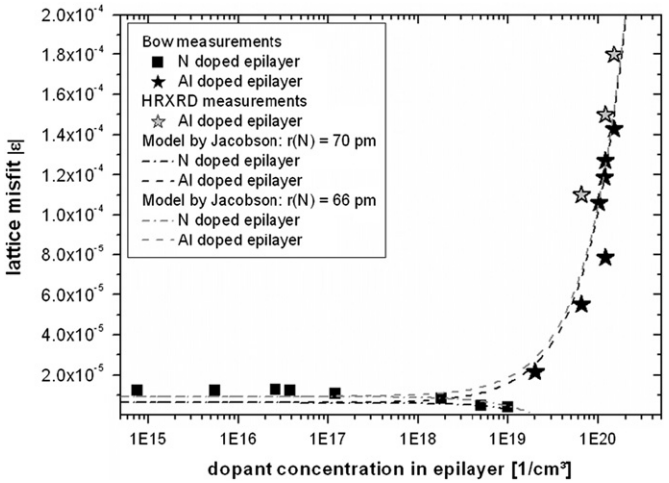

Fig. 5. Lattice misfit as a function of epilayers' dopant concentration for N (squares) and Al-doped (gray and black stars for HRXRD and curvature measurements, respectively) epilayers. Predicted values by Jacobson's model are indicated as broken lines.

For Al-doped epilayers grown on highly N-doped substrates, the experimental values of misfit, deduced from HRXRD and bow measurements, and the theoretical prediction based on Jacobson's model fit well. The misfit increases with increasing Al-concentration in the epilayer as the difference in lattice constants of highly N-doped substrate and highly Al-doped epilayer becomes more pronounced the higher the Al doping concentration of the epilayer is. The maximum misfit for Al-doped epilayers grown on highly N-doped substrates was determined as $\epsilon = -1.8\times 10^{-4}$ for $c_{Al} = 1.5\times 10^{20}$ cm^{-3}.

In the case of N-doped epilayers grown on highly N-doped substrates, a qualitative agreement between experimental data and theoretical prediction is found, i.e. the misfit between epilayer and substrate is constant at a value of $\epsilon = -1\times 10^{-5}$ for low N-doped epilayers ($c_N < 2\times 10^{17}$ cm^{-3}) and decreases further for increasing N concentration of the epilayer. The decreasing misfit with increasing N concentration of the epilayer is due to the fact that the N concentration of the epilayer is approaching the N concentration of the substrate. Perfect fitting of substrate and epilayer, i.e. negligible misfit, is found for identical N concentrations of substrate and epilayer at $c_N = 2\times 10^{19}$ cm^{-3}. In order to improve the quantitative matching between experimental misfit data and theoretical ones, the covalent radius of N was used as free fitting parameter. The best fit between experimental and theoretical misfit was found for a covalent radius of $r_N = 66$ pm. This value is slightly smaller than the literature data of r_N, which vary between 70 pm and 75 pm [13,14].

The misfit data are now used to calculate the critical epilayer thickness in conjunction with doping.

4.2. Critical epilayer thickness

In the first part of this section, the pertinent models for the prediction of critical epilayer thickness are introduced. In the

second part, we discuss whether the epilayers are (fully) strained or relaxed based on the experimental results. Finally, the experimental results will be compared with the predictions of the pertinent models.

4.2.1. Models for critical epilayer thickness

During epitaxial growth on a substrate, elastic stress builds up with increasing epilayer thickness due to the misfit between substrate and epilayer. The elastic stress can be reduced by the formation of misfit dislocations. Two pertinent models describe the formation of misfit dislocations in dependence of the epilayer thickness in conjunction with misfit between substrate and epilayer.

The model of Matthews and Blakeslee [16,17], called MB-model hereafter, assumes that threading dislocations exist in the substrate and propagate to the epilayer. The threading dislocation segment within the epilayer experiences a certain force due to the lattice misfit, which is balanced by the dislocation line tension. If the misfit induced force exceeds the force due to dislocation line tension, the formation of a misfit dislocation becomes favorable. This misfit dislocation is formed by glide of the threading dislocation segment within the epilayer, leaving behind an additional dislocation segment in the substrate–epilayer interface. The interfacial strain can only be reduced, if the Burgers vector of the misfit dislocation coincides with the in-plane lattice parameter of the interface. In the case of 4H-SiC homoepitaxy on vicinal, (0001) oriented substrates, the in-plane lattice parameter and therefore the Burgers vector of misfit dislocations is of type $\langle 11\bar{2}0 \rangle$. As the line vector of misfit dislocations needs to be within the interface, i.e. the basal plane, misfit dislocations in 4H–SiC homoepitaxial growth are so-called basal plane dislocations (BPD). Consequently, the original threading dislocation also must have an a-type Burgers vector, such dislocations are commonly known as threading edge dislocation (TED) in 4H–SiC. It is noteworthy that the dislocation density at the epilayer surface remains unchanged although misfit dislocations are formed according to the MB-model. The critical epilayer thickness h_c can be calculated based on the MB-model

$$\epsilon = \frac{b(1-\nu\cdot\cos^2\theta)}{h_c\cdot 8\pi\cdot(1+\nu)\cos\lambda}\cdot\ln\left(\frac{\alpha_c\cdot h_c}{b}\right), \tag{6}$$

with θ is the angle between Burgers and line vector of dislocation; α_c is the factor representing dislocation core, $\alpha_c = 1$; λ is the angle between the glide plane of the threading dislocation and the substrate–epilayer interface; $|b| = a = 0.308$ nm; ν is the Poisson ratio, $\nu = 0.2$ [15].

The model by People and Bean [18], called PB-model hereafter, assumes the substrate and epilayer to be initially free of dislocations. Misfit dislocations are formed by inserting a dislocation half-loop at the surface of the epilayer, followed by glide towards the substrate–epilayer interface along the strain field in the epilayer. In this case, the dislocation density at the epilayer surface increases due to the two intersection points per dislocation half loop. Based on the PB-model, the critical epilayer thickness can be calculated by Eq. (7) (using the same symbols as for MB model, a_0: in-plane lattice parameter of substrate)

$$\epsilon = \sqrt{\frac{b^2(1-\nu)}{h_c 16\pi\sqrt{2}a_0(1+\nu)}\cdot\ln\left(\frac{h_c}{b}\right)}. \tag{7}$$

4.2.2. Distinction between pseudomorphic and relaxed epilayers

The experimentally determined misfit data, deduced from HRXRD and bow measurements, as well as the dislocation densities of substrates and subsequently grown epilayers, obtained by DSE and SXRT, are now discussed in order to distinguish between pseudomorphic and relaxed epilayer growth.

The HRXRD measurements on highly Al-doped epilayers revealed that the in-plane lattice constants of substrate (a_0) and highly Al-doped epilayers (a_f) coincide exactly (compare Fig. 4a). This proves pseudomorphic growth, i.e. the epilayers are fully strained without any misfit dislocations. This finding agrees in principle with the results of Huh et al. [3] for highly Al-doped epilayers grown on HPSI substrates.

Bow measurements circumstantiated that all epilayers are bowed convexly, which agrees well with the predictions of Jacobson's model. We assume that the magnitude of curvature gives further helpful information for the distinction between pseudomorphic and relaxed epigrowth according to the following considerations: for pseudomorphic growth, it is assumed that the curvature increases steadily with increasing epilayer thickness, increasing Al concentration or decreasing N concentration of the epilayer. In the case of relaxed epigrowth, the strain within the epilayer is lowered due to misfit dislocations. Therefore, we expect the curvature of relaxed epilayers to be smaller than for fully strained epilayers, e.g. a saturation behavior might occur instead of a steady increase. For example, the curvature of the samples with low N-doped epilayers increases proportionally to the epilayer thickness (compare Fig. 3b). According to the considerations above, it is concluded that all low N-doped epilayers with a thickness up to 50 μm are fully strained. Furthermore, a steady increase of curvature with increasing Al concentration in the epilayer is observed (see Fig. 3a). Hence, the highly Al-doped epilayers are also assumed to be fully strained. The analogous observation and interpretation is valid for N-doped epilayers.

The dislocation densities of epilayers and substrates were investigated by DSE and SXRT as described in Section 3.1. Tracking of dislocations from the substrate to the subsequently grown epilayer by SXRT reveals that (i) the dislocation densities of substrate and epilayer are identical and (ii) no misfit dislocations are found at the substrate–epilayer interface. This proves again pseudomorphic growth. Furthermore, all epilayers from one growth series, i.e. epilayers grown on adjacent substrates cut from the same boule, show comparable etch pit densities and lateral distributions.

In summary, no evidence for dislocation generation is found and it is therefore concluded that all epilayers investigated within this study are fully strained.

4.2.3. Comparison of experiment and models

All pseudomorphic epilayers are displayed in Fig. 6 together with the critical thickness according to the models by Matthews and Blakeslee as well as by People and Bean. The MB model predicts smaller critical thickness than the PB model due to the smaller energetic effort for glide of a preexisting threading dislocation (MB model) compared to that for generation of a new dislocation half loop (PB model). This large deviation between the two models was also reported by Huh et al. [3].

According to the MB model, all Al-doped and N-doped epilayers are expected to contain misfit dislocations. This is in contradiction to our experimental results. Huh et al. [3] also reported that the MB model underestimates the real critical thickness of 4H–SiC homoepitaxial layers. Several explanations are given in literature: (i) the MB model describes the formation of the very first misfit dislocation [8], which is almost impossible to detect on a 3 in. SiC sample. (ii) The MB model fits well to compound semiconductors with mostly ionic bonds [19]. SiC possesses mostly covalent bondings as the electronegativities of Si and C are pretty similar. (iii) 4H–SiC homoepitaxial growth is performed in step-flow mode, which may influence the buildup of strain in the growing epilayer and hence the critical thickness. (iv) The glide of threading dislocations in the epilayer might be

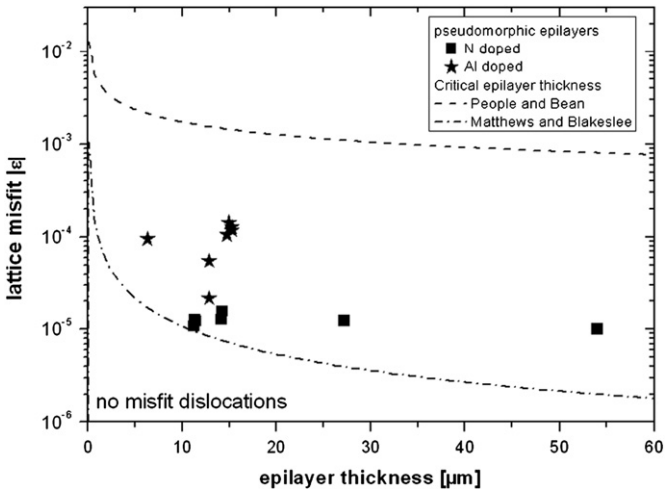

Fig. 6. Lattice misfit between substrate and epilayer versus epilayer thickness. Experimental data of pseudomorphic epilayers are shown as squares (N-doped epilayers) and stars (Al-doped epilayers). Critical epilayer thickness according to the models by Matthews and Blakeslee as well as by People and Bean are displayed as dot-pointed line and broken line, respectively.

hindered by very high Peierls stress τ_P, which must be exceeded for glide of a TED in 4H–SiC. The Peierls stress can be calculated [20] for TEDs in 4H–SiC to be $\tau_P = 560$ MPa. In summary, the discrepancy between experiment and the predictions of the MB model does not disprove the validity of MB model, but the validity of the MB model cannot be verified, too.

According to the PB model, all epilayers investigated in this study are assumed to be free of misfit dislocations, which is consistent with our experimental results. To experimentally prove the critical layer thickness predicted by the PB model (about 100 µm for $\epsilon = -2 \times 10^{-4}$), sufficiently thick epilayers would be needed, but the growth of such thick, high quality epilayers is very difficult. In contrast to the basic assumptions of the PB model, 4H–SiC substrates and epilayers contain typically several 10^4 dislocations/cm^2. It is therefore questionable if the PB model applies to 4H–SiC in general, as it seems very unlikely that 4H–SiC homoepitaxial layers are only able to relax by generation of additional dislocation halfloops although (threading) dislocations are present in the material.

Generally spoken, the MB and PB models might fail to describe the relaxation mechanism of 4H–SiC properly, as other authors already reported that the relaxation of homoepitaxial layers is linked to the formation of stacking faults. This is very likely due to the low stacking fault energy in (4H-) SiC [21]. Huh et al. [3] have proven the existence of dislocation halfloops and stacking faults in relaxed, heavily Al-doped epilayers (with $c_{Al} = 3.3 \times 10^{20}$ cm^{-3}; corresponding to $\epsilon = -4 \times 10^{-4}$) with 10 µm thickness. Similarly, Jacobson et al. [5] have shown that stacking faults occur in low N-doped epilayers ($c_N = 3 \times 10^{15}$ cm^{-3}; epilayer thickness 30 µm) grown on highly N-doped substrates. The epilayer thickness, at which the formation of stacking faults and misfit dislocation begins, is much smaller than the predicted critical epilayer thickness according to the PB model. The experimental reports of Huh et al. [3] and Jacobson et al. [5] suggest that the formation of stacking faults plays an important role for the relaxation of 4H-SiC epilayers. If stacking faults really govern the strain relaxation in 4H–SiC homoepitaxial layers, they need to be included to the models for critical epilayer thickness.

5. Conclusions

The lattice misfit in 4H–SiC homoepitaxial growth on highly N-doped, commercial substrates is induced by doping. The impact of the dopant (N and Al) and its concentration on lattice parameters and misfit is investigated experimentally by HRXRD and bow measurements and theoretically by Jacobson's model. The bow measurements are suitable for a quick and easy check regarding the strain in the epilayer, even for N-doped epilayers grown on N-doped substrates. Furthermore, it has the potential to become a standard in-line measurement tool for the production of epilayers and devices. The pertinent models for critical epilayer thickness cannot describe satisfactorily the critical epilayer thickness for 4H–SiC homoepitaxy. Further development of these models is needed with respect to stacking faults.

Acknowledgments

This work was part of the KoSiC project funded by the Bavarian Research Foundation (BFS) under contract number AZ-720-06. We acknowledge the Synchrotron Light Source ANKA for provision of beamtime at the TOPO-TOMO beamline and we would like to thank the beamline team and Dr. A.N. Danilewsky (Crystallography, University of Freiburg, Germany) for support of the measurements and helpful discussion of the results.

References

[1] J.P. Bergman, H. Lendenmann, P.A. Nilsson, U. Lindefelt, P. Skytt, Materials Science Forum 353–356 (2001) 299–302.
[2] R.S. Howell, S. Buchoff, S.V. Campen, T.R. McNutt, H. Hearne, A. Ezis, M.E. Sherwin, R.C. Clarke, R. Singh, IEEE Transactions on Electron Devices 55 (2008) 1816–1823.
[3] S.W. Huh, H.J. Chung, M. Benamara, M. Skowronski, Journal of Applied Physics 96 (2004) 4637–4641.
[4] H.J. Chung, M. Skowronski, Journal of Crystal Growth 259 (2003) 52–60.
[5] H. Jacobson, J. Birch, C. Hallin, A. Henry, R. Yakimova, T. Tuomi, E. Janzen, U. Lindefelt, Applied Physics Letters 82 (2003) 3689–3691.
[6] R.S. Okojie, T. Holzheu, X. Huang, M. Dudley, Applied Physics Letters 83 (2003) 1971–1973.
[7] C. Hecht, B. Thomas, W. Bartsch, Material Science Forum 527–529 (2006) 239–242.
[8] L.B. Freund, S. Suresh, Thin Film Materials: Stress, Defect Formation and Surface Evolution, second ed., Cambridge University Press, 2009.
[9] B. Kallinger, S. Polster, P. Berwian, J. Friedrich, G. Müller, A.N. Danilewsky, A. Wehrhahn, A.-D. Weber, Journal of Crystal Growth 314 (2011) 21–29.
[10] A.N. Danilewsky, R. Simon, A. Fauler, M. Fiederle, K.W. Benz, Nuclear Instruments and Methods in Physics Research B 199 (2003) 71–74.
[11] B. Kallinger, B. Thomas, S. Polster, P. Berwian, J. Friedrich, Materials Science Forum 645–648 (2010) 299–302.
[12] B. Kallinger, et al., to be published.
[13] S. Hauptmann, G. Mann, Stereochemie, Spektrum Akademischer Verlag, Heidelberg, 1996.
[14] J.E. Huheey, E.A. Keiter, R.L. Keiter, Anorganische Chemie, third ed., Walter de Gruyter, 2003.
[15] K. Kamitani, M. Grimsditch, J.C. Nipko, C.-K. Loong, M. Okada, I. Kimura, Journal of Applied Physics 82 (1997) 3152.
[16] J.W. Matthews, A.E. Blakeslee, Journal of Crystal Growth 27 (1974) 118–125.
[17] J.W. Matthews, Journal of Vacuum Science and Technology 12 (1975) 126–133.
[18] R. People, J.C. Bean, Applied Physics Letters 47 (1985) 322–324.
[19] R. Hull, J.C. Bean, Critical Reviews in Solid State and Materials Sciences 17 (1992) 507–546.
[20] D. Chidambarrao, G.R. Srinivasam, B. Cunningham, C.S. Murthy, Applied Physics Letters 57 (1990) 1001.
[21] M.H. Hong, A.V. Samant, P. Pirouz, Philosophical Magazine A 80 (2000) 919–935.